Characterization of the In-vitro Dynamic Behavior of the Human Thoracic Spine in Flexion

Francisco J. Lopez-Valdes, Sabrina H. Lau, Patrick Riley, Richard W. Kent

Abstract The goal of this study is to characterize the *in vitro* dynamic response of the human thoracic spine undergoing flexion in the sagittal plane. Eight human functional spinal units (FSU) were harvested from four donors (7, 15, 48 and 52 years old). FSU consisted of three contiguous vertebrae (T2-T4 and T7-T9), representing two different regions along the thoracic spine. All ligaments were preserved intact in the preparation of the tissue, with the exception of the inter-transverse ligaments. Specimens were exposed to a battery of tests using a customized fixture designed to induce a moment at both ends of the specimens. Fung's quasi-linear viscoelastic (QLV) formulation was used to model the relationship between the moment applied to one vertebra and the subsequent relative motion with respect to a contiguous one. In general, the upper thoracic FSU (T2-T4) exhibited a more compliant behavior than the mid-thoracic segments (T7-T9) regardless of age. It was also observed that the instantaneous elastic response of the older specimens was stiffer than the one calculated for the younger ones.

To the knowledge of the authors, no characterization of the dynamic flexural behavior of the thoracic spine has been published to date. Therefore, despite the small sample size, the data included in the study can assist in developing more biofidelic models of the human thoracic spine and to benchmark existing ones.

Keywords Pediatric Biomechanics, Post Mortem Human Surrogate tests, Quasi-Linear Viscoelasticity, Thoracic Spine, Bending.

I. INTRODUCTION

Despite the kinematics of the head and neck as well as the interaction between the occupant's torso and the restraints are strongly influenced by the dynamics of the thoracic spine [1], little experimental data on the kinematics and dynamics of the human thoracic spine are available.

This paucity of data is associated with the growing body of literature pointing out the existing differences in the kinematics of the torso between human volunteers or Post Mortem Human Surrogates (PMHS) and Anthropomorphic Test Devices (ATD). Recent studies combining full sled tests and computer simulations have found significant differences in the magnitudes of the acceleration at T1 and the neck loads between Anthropomorphic Test Devices (ATD), volunteers and cadavers [2-5]. Other studies have shown similar findings in pediatric ATD [6-11].

The vast majority of the published literature on the mechanical behavior of the thoracic spine belongs to the field of orthopedics and orthotics. Although these studies are clinically relevant [11-12], they are of limited interest in the prevention of motor-vehicle related injuries. A few studies have attempted the mechanical characterization of the cadaveric thoracic spine in bending [13-14] only in quasi-static conditions. A more recent study measured the *in-vivo* 3D kinematics of the human thoracic spine, but again in quasi-static conditions [15]. The study showed that quasi-static flexion and extension were relatively pure plane motions, accompanied by slight axial rotation. Methods such as the instantaneous helical axis (IHA) have been used to characterize the 3D kinematics of several functional spinal units (FSU) in axial rotation, lateral bending and flexion/extension in preserved [16] and fresh PMHS [17], without investigating the material properties of the specimens.

Thus, the field is lacking experimental data on the dynamic behavior of the human thoracic spine that can assist in the development of computer models of the spine at relevant strain rates. This is recognized in the target priorities for the phase II of the development of the GHBMC model [18]. In what can be considered as

F.J Lopez-Valdes, PhD, is a Marie Curie Fellow at the Technologies and Systems for Automotive Safety laboratory of the University of Zaragoza (+34976762611; fjlv@unizar.es). S. H. Lau, MSc, lectures at Clemson University. P. Riley, PhD, and R. Kent, PhD, are at the Center for Applied Biomechanics of the University of Virginia. The work described in this paper was completed while the four authors were at the Center for Applied Biomechanics of the University of Virginia.

one of the most advanced human body models, the capability of the model to predict spinal injuries is ranked as 3-4 in a scale from 0 to 6, indicating insufficient model detail partially caused by the unavailability of test data. In the case of pediatric subjects, the need for additional data to generate constitutive models of the pediatric spine is even more pressing.

The absence of constitutive data for the pediatric intervertebral discs, ligaments and synchondroses of the cervical spine has led researchers to use scaled adult data [19-23]. However, the significant differences in the kinematics of the cervical and thoracic spine existing between children and adults questions the approach of scaling adult data to approximate the behavior of pediatric occupants [24-25]. Therefore, it is necessary to develop constitutive models of the pediatric spine that can be implemented in computational models of children. As recognized in [26], the design and performance specifications of future pediatric ATD will be based largely on finite element and multibody models. To date, there are still many unanswered questions regarding the structural dynamic behavior of the developing spine and the material properties of pediatric spinal tissue.

Thus, the goal of this study is to provide a model of the structural behavior of the thoracic spine in dynamic bending that can assist in the development of human body models. To this end, the paper shows results from eight specimens corresponding to two different levels of the thoracic spine. These results will be used to investigate the following two hypotheses:

- The stiffness of the thoracic spine remains constant within the same subject along the whole length of the subject's spine.
- There is no difference in the stiffness of the developing thoracic spine and the mature one in dynamic bending.

II. METHODS

Test specimens

A total of eight Functional Spinal Units (FSU) were harvested from four donors (two pediatric, two adults). The anthropometry and general characteristics of the donors are shown in Table I. For the purpose of this study, a FSU was defined as the specimen formed by three vertebral bodies, the corresponding two inter-vertebral discs and the ligaments connecting these structures. Specimens were kept frozen after harvesting and thawed 24 hours prior to testing. All the ligaments (supra-spinous (SSL), inter-spinous (ISL), flavum (LF), posterior longitudinal (PLL), anterior longitudinal (ALL)) were preserved during the preparation of the specimens with the exception of the inter-transverse ligaments. Two FSU were obtained from three of the donors: T2-T4 and T7-T9. Specific information of the geometry of the FSU can be found in the Appendix. The extraction, preparation and testing of the specimens were done in compliance with the Protocol for the Handling of Biological Material [27] and approved by the University of Virginia – Center for Applied Biomechanics Oversight Committee.

TABLE I
GENERAL CHARACTERISTICS OF THE PMHS

Subject	Gender	Age	Stature (cm)	Weight (kg)
F470	Female	7	119	27
M485	Male	15	163	50
M319	Male	52	179	77
M320	Male	48	168	68

The proximal and distal vertebrae of each FSU were embedded into cement (Fast Cast, polyurethane isocyanate, Goldenwest Inc., CA, USA). A custom-made potting fixture was used to ensure that the two cement blocks were aligned without inducing any initial stress in the specimens. The center of the potted vertebral bodies was approximately positioned at the center of the cement block. To preserve the hydration of the ligamentous structure they were wrapped in gauze soaked in saline solution. The specimens were submerged in a temperature-controlled water bath set at 37.1 degrees Celsius for at least 30 minutes immediately prior to testing.

Test setup

A custom-made fixture specifically designed to induce a bending moment in a section of the spine was attached to a servohydraulic testing machine (INSTRON 8874 Axial-Torsion Fatigue Testing Systems, Norwood,

MA, USA). The fixture was driven by the vertical motion of the piston of the machine, transforming the piston linear motion into a rotation of two cups through a mechanical linkage, consisting of two aluminum arms joined by a low-friction rotational bearing. The vertical arm was attached to the crosshead of the testing machine by a low-friction linear bearing and translated freely in the horizontal direction. The cups were supported by two cup-holders that could translate with negligible friction in the horizontal plane of the table of the test machine. A global coordinate system (GCS) rigidly attached to the table of the test machine was defined as shown in Fig. 1.

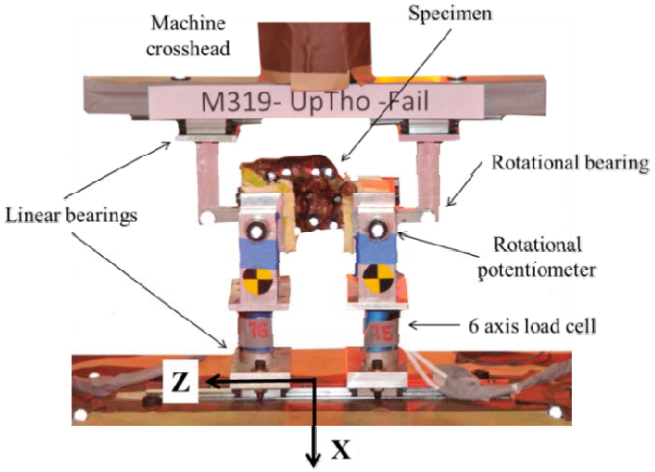

Fig. 1. Schematic showing the test setup, instrumentation used and positioning of the test specimen..

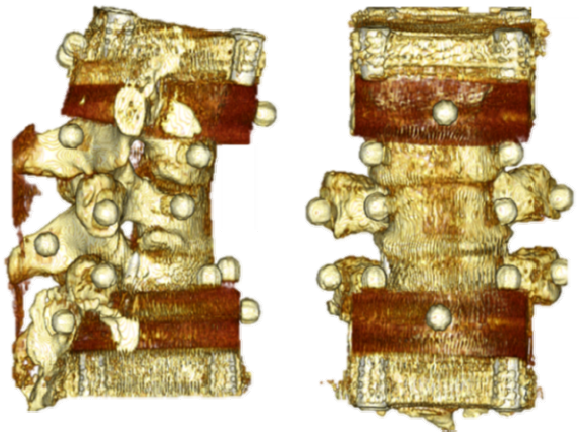

Fig. 2. CT image of one specimen showing the position of the retroreflective markers on the vertebrae.

First, each specimen was exposed to a battery of 50 cycles at 1 Hz sinusoid with different amplitudes to precondition the tissue and achieve a steady-state behavior. Next, a series of five dynamic ramp and 60-second hold tests of varying amplitudes were applied to the specimens (D1-D5). The amplitude of the ramps was chosen to avoid causing any damage to the tissue and the maximum amplitude reached during the dynamic tests was similar to that reached during the preconditioning of the tissue. The piston of the test machine moved upwards at a nominal rate of 100 mm/s. Table II summarizes the test matrix as well as the machine input values of each of the tests. The values of the amplitudes presented in the table correspond to the rotation of the cups as measured by the rotational potentiometers.

TABLE II
TEST MATRIX

Specimen		Preconditioning	D1	D2	D3	D4	D5
	Freq (Hz)	# cycles/ Amplitude (deg)	Amplitude (deg)	Amplitude (deg)	Amplitude (deg)	Amplitude (deg)	Amplitude (deg)
F470-T2T4	1	10/0.65, 10/1.35, 30/1.89	0.63	0.93	1.22	1.54	1.87
F470-T7T9	1	10/0.59, 10/1.17, 30/2.00	0.61	0.89	1.15	1.37	1.61
M485-T2T4	1	10/1.04, 10/2.27, 30/3.39	0.87	1.41	1.95	2.54	3.18
M485-T7T9	1	10/1.09, 10/2.33, 30/3.44	0.85	1.42	2.00	2.64	3.32
M319-T2T4	1	10/1.14, 10/2.25, 30/3.35	0.96	1.53	2.13	2.69	3.24
M319-T7T9	1	10/1.18, 10/2.43, 30/4.64	0.79	2.04	3.35	3.98	4.59
M320-T2T4	1	10/1.24, 10/2.36, 30/3.41	1.10	1.75	2.43	2.96	3.46
M320-T7T9	1	10/1.07, 10/2.01, 30/2.97	0.87	1.43	2.04	2.57	3.10

Instrumentation

The motion of the vertebrae was tracked using an 8-camera Vicon MX™ system operating at 1000 Hz. The system recorded the motion of retroreflective targets within the camera's collective viewing volume. Four

targets were glued onto each vertebra to allow for the reconstruction of their 3D motion (Fig. 2). A local coordinate system located at the center of the vertebral body was defined for each vertebra [28]. Using geometric information from CT images, the position and attitude of the local coordinate system can be related to the position of the four retroreflective targets. Finally, the motion of each vertebra can be determined with respect to an inertial global coordinate system (GCS) that coincides with the base of the test machine [29]. Given the characteristics of the system, the motion analysis was restricted to the XZ plane as shown in Fig. 1. The motion capture system permitted measuring the distances between the local coordinate system of each vertebra, needed to estimate the moments and forces experienced by the specimen according to the detailed methodology included in the Appendix.

In addition to the optical instrumentation, two load cells (Implantable Fibula, Model No. 5024J, Robert A. Denton, Inc. MI, USA) measured the reaction forces and moments in the three coordinate axes at the support of the cups. The longitudinal axis of the load cells intersected perpendicularly with the axis of rotation of the cups. The rotation of the cups was measured by two rotational potentiometers. Instrument data were collected at 10000 Hz using a DEWE-2600 (Dewetron Inc., Wakefield, RI, USA) data acquisition system. The data were filtered using 4-channel Butterworth low-pass CFC100 (rotational potentiometers) and CFC1000 filters (forces and moments).

Quasi-linear Viscoelastic (QLV) formulation

A quasi-linear viscoelastic model (QLV) was proposed to characterize the dynamic behavior of the thoracic FSU. The QLV formulation has been applied successfully to describe the transient non-linear behavior of biological tissues [29] as well as of structures as a whole [30-34]. The selected QLV formulation relates the calculated specimen angle to the generated bending moment, according to Eq. (1):

$$M(t) = \int_{-\infty}^{t} G(t-\tau)\left(\frac{\partial M_e(\alpha\alpha}{\partial \alpha}\right)\left(\frac{\partial \alpha(\tau)}{\partial \tau}\right)d\tau \quad (1)$$

where M(t) is the moment generated, G(t) is the generalized relaxation function, α(t) is the angle rotated and $M_e(\alpha)$ is the function describing the moment response to a step increase in rotation. The formulation of the method is included in the Appendix. The angle α(t) was obtained combining the measurement given by the two rotational potentiometers as indicated in Fig. 3 and in Equation (2).

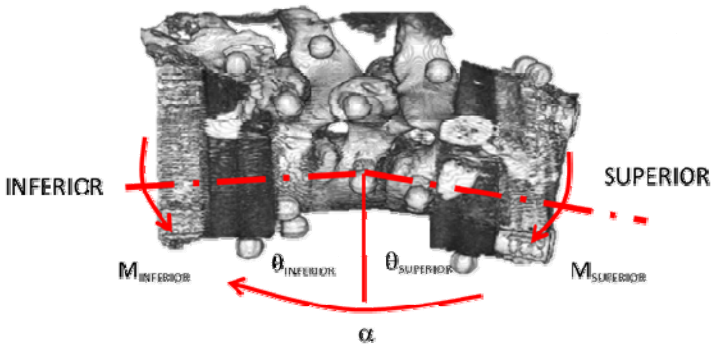

Fig. 3. Schematic of the FSU showing the calculation of the relative angle between the two distal vertebrae

$$\alpha = \theta_{superior} + \theta_{inferior} \quad (2)$$

The methodology followed to calculate the values of $M_{INFERIOR}$ and $M_{SUPERIOR}$ is detailed in the Appendix. The parameters of the model were optimized simultaneously in the D3, D4 and D5 dynamic ramp-and-hold tests to minimize the sum of square errors between the model-predicted moment and the measured one. The results from the experiments D1 and D2 were not included to improve the fit of the model to greater angle amplitudes. The optimization used a genetic algorithm scheme implemented in MATLAB that increased the likelihood of finding a global minimum of the problem. In the optimization problem, the earlier response of the specimens was assigned a greater weight than the long-time response to improve the prediction of the transient response.

III. RESULTS

Preconditioning and rate effects

Specimens were preconditioned for 50 cycles at 1 Hz of increasing amplitude up to, approximately, the maximum target experimental amplitude (D5). Preconditioning was applied until there was not significant variation between two consecutive load peak values. The behavior of the specimen M320 T2-T4 was substantially different from any of the other specimens, showing important differences in the shear forces between the distal and proximal end. This specimen was removed from further analysis. Fig. 4 shows the response of one pediatric and one adult specimen during preconditioning.

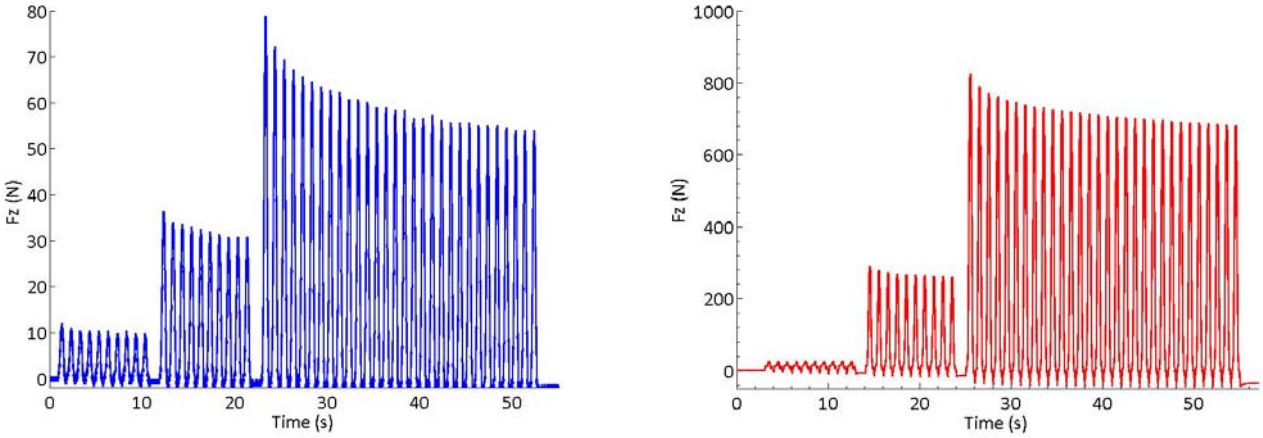

Fig. 4. Distal force vs. time history plots of pediatric specimen F470 T7-T9 (left) and adult specimen M320 T7-T9 (right) showing the effects of preconditioning on the response of the specimens.

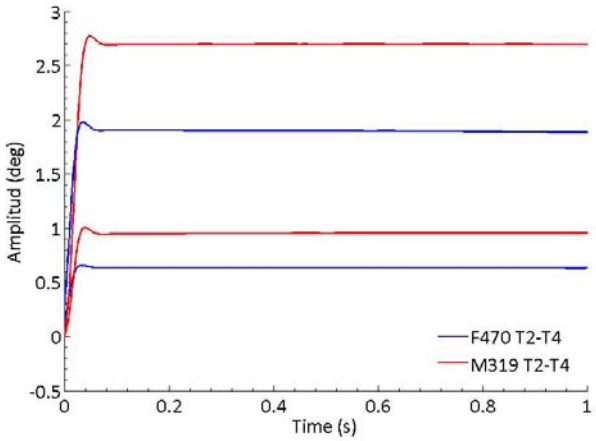

Fig. 5. Comparison between the effective angular rate obtained in the tests of the smallest pediatric specimen F470 T7-T9 (blue) and of the adult specimen M320 T7-T9 (red), in the slowest (D1) and fastest (D5) loading conditions.

The test fixture was designed to transform the longitudinal translation of the crosshead of the axial tensile machine into the rotation of the distal and proximal ends of the specimens. Due to this design, the effective rotation and angular rate applied to the specimens depended on the size of the specimen. Given the rate-dependent nature of most biological tissues, it was necessary to ensure that the angular rates applied were comparable across specimens. Fig. 5 illustrates the similar angular rate between a pediatric (F470) and an adult (M320) specimen. In this section of the spine (T2-T4), angular rates varied between 19.9 deg/s (D1) and 56.57 deg/s (D5) in the case of the smallest specimen (F470) and between 25.77 deg/s (D1) and 57.53 deg/s (D5) in one of the adult specimens. Similar values were observed in the other spinal segment and for the other specimens. No macroscopic changes or failure were observed in any specimen during preconditioning.

Curve fits

The QLV model was fitted to the experimental data corresponding to the D3, D4 and D5 amplitudes, as these tests were more relevant to the magnitudes that can be observed in a high-speed impact.

The QLV formulation did not describe satisfactorily any of the upper sections of the adult specimens. Thus,

the corresponding parameter values are not included in this study. Adult specimen M319 exhibited a behavior that could not be captured by the equation form proposed for the instantaneous elastic response (see Appendix, Eq. 4). Fig. 6 zooms into the first 100 ms of the obtained average moment in the different amplitude experiments D2-D5. The curves shown in Fig. 6 indicate that an exponential form was not appropriate to describe the results observed, as the stiffness of the D4 curve (green) was higher than the D5 one (blue). Similar behavior was found in the first 20 ms for smaller amplitudes. As for specimen M320, a completely different behavior was observed between the two ends of the specimen even during preconditioning and therefore the results from this specimen were discarded.

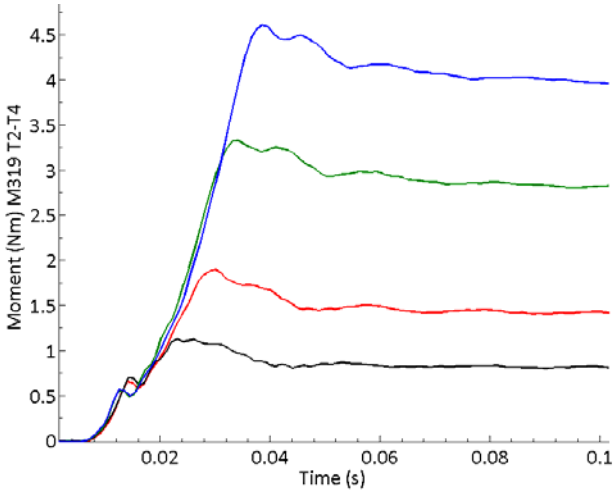

Fig. 6. Time-history of the calculated average moment (M_{ave}) of the upper thoracic section of specimen M319.

For the remaining specimens, the coefficients obtained after solving the optimization problem are shown in Table III. Fig. 7 shows the comparison between the QLV model-predicted moment (M_{est}) and the measured one (M_{ave}) for one of the pediatric specimens and one of the adults. The rest of the curves showing the model fit to the experimental data are included in the Appendix for visual inspection (Fig. A5 – Fig. A7).

The results presented in Fig. 7 and in Fig. A5-Fig. A7 show that the QLV formulation approximated correctly the moment peak and the relaxation response of the specimens.

TABLE III
COEFFICIENT VALUES OF THE QLV MODEL OF THE HUMAN THORACIC SPINE.

	β_1 (s)	β_2 (s)	β_3 (s)	G_1	G_2	G_3	G_∞	A	B	R^2
F470-T2T4	0.993	8.934	114.231	0.052	0.024	0.559	0.365	13.117	0.018	0.635
F470-T7T9	0.549	1.073	106.891	0.169	0.081	0.549	0.201	3.131	0.078	0.784
M485-T2T4	0.022	9.993	78.158	0.054	0.091	0.327	0.528	10.683	0.056	0.785
M485-T7T9	0.019	8.747	92.104	0.010	0.059	0.435	0.496	9.711	0.080	0.884
M319-T7T9	0.912	9.969	81.030	0.020	0.069	0.437	0.475	0.327	0.343	0.682
M320-T7T9	0.051	9.450	98.759	0.003	0.117	0.277	0.603	2.180	0.345	0.788

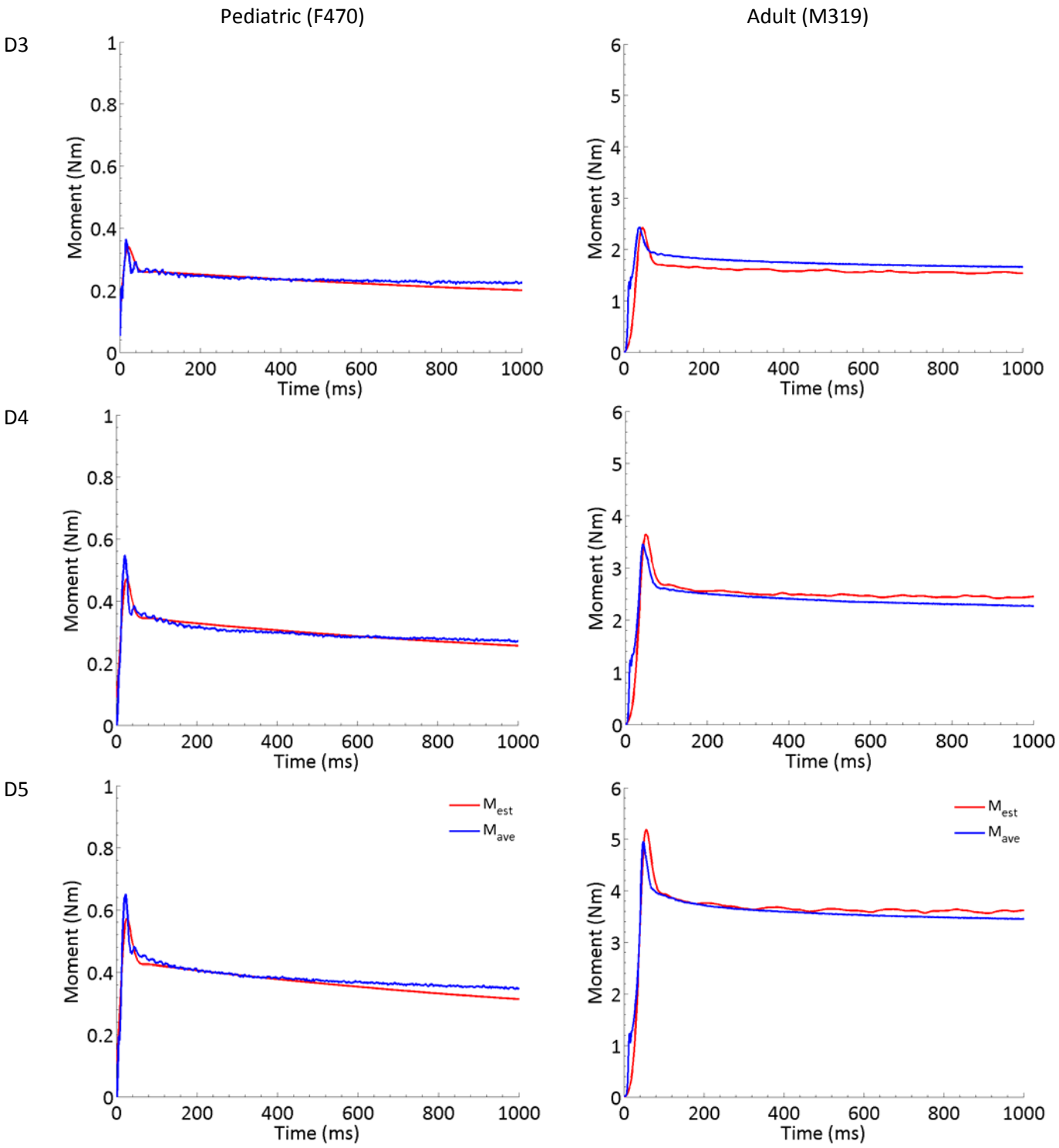

Fig. 7. Comparison between the predicted moment using the QLV model (red) and the measured experimental moment (blue). Results for the F470 T7-T9 (pediatric specimen) are shown in the left column. Right column shows the results obtained for the M319 T7-T9 (adult specimen). Note the different Y axes scales between specimens. All results are included in the Appendix.

Apart from visual inspection, the goodness of fit of the model was assessed using the coefficient of determination R^2 (values also included in Table III). In general, results obtained for the middle section of the thoracic spine showed a higher goodness of fit than the ones obtained for the upper section. In the case of specimen M319-T7T9, the goodness of fit for the amplitude D3 was very low (R^2=0.316), but the visual inspection of the estimated curves (see Appendix) and the goodness of fit obtained for the other two amplitudes (R^2= 0.804; R^2= 0.926) were considered to be a good description of the response of the specimen.

Stiffness change along the thoracic spine

The first hypothesis to be evaluated in this paper was whether the stiffness of the thoracic spine remained constant in the cephalocaudal direction. To that end, the instantaneous elastic response of the upper and middle sections of specimens F470 and M485 were plotted and compared to each other. Fig. 8 shows the results of the comparison. Solid blue curves are the instantaneous elastic response of the T7T9 section of each specimen. The instantaneous elastic response of the T2T4 section is shown in solid red. The angle amplitude for the comparison (10 degrees) was chosen arbitrarily but the magnitude was relevant for the amount of rotation that can be seen in frontal impacts [17]. Both specimens showed a stiffer response of the lower thoracic spine compared to the upper section. To quantify these effects, a coefficient κ was defined as the proportionality constant that related the instantaneous elastic response of both thoracic sections, minimizing the distance between the two curves. The coefficient κ was defined to provide an approximation of the relationship between the stiffness of different spinal sections. The value of the coefficient calculated from the experiments is shown in Table IV. The coefficient was obtained only for specimens F470 and M485 as no data were available from the other two specimens.

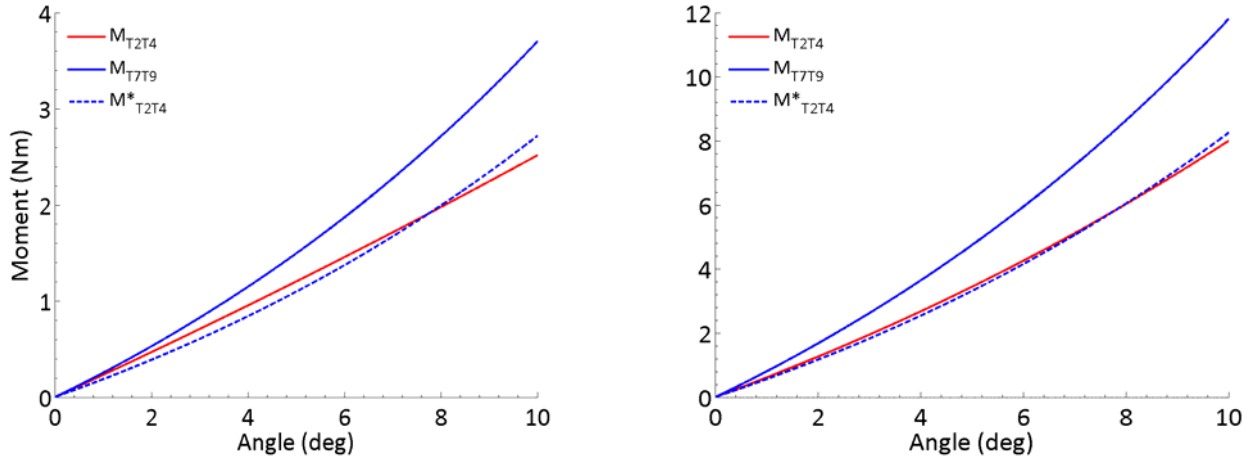

Fig.8 Comparison of the T2T4 (solid red) and T7T9 (solid blue) instantaneous elastic response of specimen F470 (left) and M485 (right), up to 10 degrees. Blue dotted lines are the approximation of the instantaneous elastic response of T2T4 given by applying the coefficient κ to the instantaneous elastic response of T7T9.

TABLE IV
RELATIONSHIP BETWEEN THE INSTANTANEOUS ELASTIC RESPONSES OF THE TESTED FSU

	F470	M485	M319	M320
κ	0.73	0.70	NA	NA

The blue dotted lines in Fig. 8 represent the approximation to the T2T4 instantaneous elastic response given by applying the coefficient κ to the T7T9 instantaneous elastic response.

Thoracic spinal stiffness change with age

As for the hypothesis assuming that the stiffness of the thoracic spine remained constant through development, the QLV model obtained for the T7T9 allowed comparing the instantaneous elastic responses of the four specimens, which provided a comparison for a 7-52 age range. The comparison is shown in Fig. 9 for the same angle magnitude of 10 degrees used in the previous section.

The instantaneous elastic response of specimen M320 T7T9 was found to be the stiffest one, followed by specimen M319, but only for larger rotation amplitudes. At smaller values of the rotation angle, the response of subject M485 was stiffer than the one exhibited by specimen M319. Finally, the youngest specimen F470 (7 YO) demonstrated the most compliant behavior of the tested specimens.

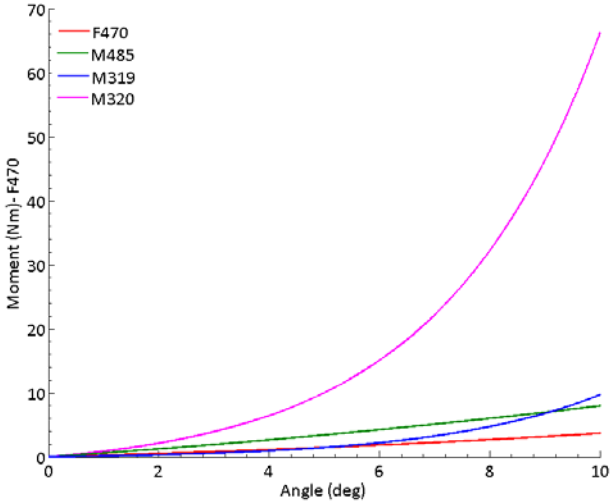

Fig. 9. Comparison of the instantaneous elastic responses of the four T7T9 specimens showing increasing stiffness with increasing age.

IV. DISCUSSION

This study characterized the dynamic behavior of two different sections of the thoracic spine in bending. Instead of analyzing the individual responses of each of the flexible components of the spine (ligamentous structures, joint capsules, intervertebral discs) the study adopted a more general approach in which the thoracic sections were addressed as single structures. Therefore, the results reported in the paper can be understood as a description of the effective bending behavior of the thoracic spine rather than a material model.

The development of human body models to represent the dynamic behavior of occupants during crashes requires the availability of experimental data to benchmark and optimize the response of the model. Although the resulting angular rates used in this study (0.3-1.3 rad/s) are smaller than the ones that can be expected in a 40 km/h frontal impact (around 10 rad/s measured at T1), these tests constitute, to our knowledge, the first *in vitro* dynamic bending tests of the human thoracic spine. Even if the number of specimens is too low to consider the question of the characterization of the flexion of the human thoracic spine completely solved, they provide the first available relationship between the mechanical behavior of different sections of the human thoracic spine in bending. In addition, future research will benefit from the results provided here to guide the experimental design of subsequent experiments. For instance, the smallest amplitudes (D1, D2) used in this study resulted in very noisy responses that could not be adequately described by the QLV model and were discarded. It is advised that future testing makes use of more representative angles, considering the tolerance limits for the moment presented in [36-37]. Failure of the specimens in bending at the rates used in this study was found at around 17 degrees for adult FSU [36]. A summary of the injuries that can be expected at these angles is also provided in [36].

The QLV formulation was applied successfully to describe the mechanical behavior of six out of the eight original specimens. The remaining two presented mechanical responses that could not be modeled under this approach. Results from the upper section of specimen M319 were shown in Fig. 6. These curves indicate a softening of the specimen with increasing rotated angle. Although no further analyses were done, this behavior may suggest microstructural damage during testing. Similar reasoning can be used to explain the extremely different moments found in the two ends of specimen M320 T2T4. In this case, even during the smallest amplitude cycles in the preconditioning phase, the specimen showed a very different behavior at T2 and at T4. These differences were only identified post-test. Given the difficulties found during testing, it is recommended to perform a progressive preconditioning-testing process. Instead of preconditioning the samples up to the maximum intended amplitude before running the battery of step and hold tests, we suggest to precondition the specimen up to a certain magnitude and to perform the step and hold test for that magnitude. Using this approach will help to clarify whether the specimens can be damaged during preconditioning.

Despite these difficulties, the stiffness of two different sections along the spine could be compared in

specimens F470 and M485. Both subjects showed a stiffer behavior of the lower section (T7T9) of the thoracic spine. There are no data available in the literature with which to compare, but this information in itself might be useful in the setup of multibody models of the human spine. It is significant to highlight the good agreement found in the prediction of the proportionality constant κ. The change in the bending stiffness of the two FSU within the same subject can be likely attributed to the geometrical changes occurring along the length of the thoracic spine. Thoracic vertebrae grow in height and width in the cephalocaudal direction, contributing to increased stiffness of the structure. Also, a change in the orientation of the facet joints that tend to be more vertical at lower levels of the thoracic spine has been reported in the literature [38]. The geometrical changes of the vertebrae along the spine of the FSU included in the study are shown in Table A2 and Table A3 in the Appendix.

The tests presented here also served to evaluate if there is a change in the stiffness of the spine with age. As expected, older subjects exhibited a stiffer behavior. Since the bending behavior of the specimens was studied as an effective behavior, it is clear that the size of the specimens is influencing these results. That reason might explain the similarities found between the 15 YO specimen (M485) and the 52 YO (M319). The older specimen was more compliant than the younger one up to approximately 9 degrees in which the slope of the moment vs. angle curve started to increase faster than in the adolescent specimen. The youngest specimen exhibited the most compliant behavior of the four specimens. Developmental changes (ossification of vertebrae, changes in the angle of the facet joints, increase of vertebrae height, development of the annulus fibrosus of the intervertebral discs) have been suggested often in the literature as the cause for differences in spinal range of motion between children and adults [23, 39-41].

Structural models of the cervical and lumbar spine

Although there is plenty of literature discussing the non-linear behavior of ligaments, including those of the spine, it is difficult to find studies characterizing the structural behavior of sections of the spine. Most of the papers reporting results from spinal FSU do not attempt to provide a model of the behavior but to describe the characteristics at failure. In those instances in which a model is provided, the time component of the behavior is generally ignored. Thus, the comparison between these studies and ours is limited.

One study characterizing the bending behavior of the pediatric cervical spine in the sagittal plane compared two age groups (2-4 years old and 5-12 years old) including 10 specimens [42]. There were not significant differences observed in the average stiffness of the pediatric neck for a quasi-statically applied moment ranging between -2.4 Nm (extension) and 2.4 Nm (flexion). The reported stiffness was 0.041±0.007 Nm/deg. At approximately the same moment amplitude and for the youngest specimen (F470), the QLV model developed here predicted a stiffness of 0.251 Nm/deg in the upper section and of 0.329 Nm/deg in the mid-section of the thoracic spine. Both values were substantially greater than the ones reported for the cervical spine by Ouyang and coauthors [42]. However, it seems logical that the thoracic spine is stiffer than the cervical. In addition, the cervical data were obtained in quasi-static conditions while our data corresponds to dynamic tests. A different study exposed cervical FSU from mature animal surrogates (caprine model) to dynamic bending in the sagittal plane up to 2.0 Nm [43]. The study reported stiffness values between 0.40 Nm and 0.44 Nm, depending on the size of the animal. These results were used to obtain scaling factors for the bending stiffness between pediatric and adult human specimens. Other studies investigating the structural properties of the adult human spine have reported stiffness values raging between 0.42 Nm/deg and 1.46 Nm at failure, depending on gender and cervical level [44,45].

As for the lumbar spine, a study recognizing the viscoelastic behavior of the lumbar soft tissues provided an estimation of the average bending stiffness of the lumbar spine ranging between 4.66 Nm/deg and 5.22 Nm/deg [46] for flexion values around 11 degrees and depending on the rate at which the moment was applied. A similar study subjecting lumbar FSU to quasi-static bending up to 1.0 degree reported average stiffness values around 4.21 Nm/deg [47]. As was expected, these values were greater than the previous ones reported for the cervical and thoracic spine.

Limitations of the study

The study presents two major limitations: the reduced number of specimens tested and whether these specimens were representative of their respective age groups. The first limitation precluded the use of any statistical method to check the significance of the hypotheses under study. As for the second one, in the absence of any other data, it is difficult to assess the relevance of this limitation. Although the testing methodology used in [37] differs substantially from the one used here (since the loading mechanism was vertical deceleration), the magnitude of the resulting failure moments are comparable to those reported in [36]. Even if [37] only adds data from three additional subjects, and given that the specimens discussed in [36] are the same ones analyzed here, it is worth mentioning that reported results are within the same order of magnitude.

It should be pointed out that the response of the thoracic spine is influenced by the surrounding structures. Therefore, the mechanical behavior of these component tests is not likely to be directly transferable to the case of a whole human body [14]. Nevertheless, modeling the structural behavior of selected thoracic sections has helped to understand the differences in stiffness along the spine as well as the differences in its mechanical behavior with age. These results can be useful in the development of numerical models of the human spine and provide data to benchmark the biofidelity of these models.

V. CONCLUSIONS

The present study presents data from eight human functional spinal units (FSU) that were harvested from four donors (7, 15, 48 and 52 years old). FSU consisted of three contiguous vertebral bodies (T2-T4 and T7-T9), representing two different regions along the thoracic spine. Fung's QLV method was used to model the relationship between the angle rotated by the FSU and the resulting bending moment. The study discusses the limitations found in the experimental design and the influence of these limitations in the results. A QLV formulation was able to describe the bending dynamic behavior of the thoracic FSU in six out of the eight initial specimens. This formulation allowed comparing the stiffness of different sections of the thoracic spine of the same subject and across different ages. It was found that the T2T4 section was more compliant than the T7T9. Older specimens exhibited a stiffer response than younger ones. To the knowledge of the authors, these are the first experimental results characterizing the dynamic bending behavior of thoracic FSU.

VI. ACKNOWLEDGEMENTS

The authors would like to thank Matt Kindig, Mark McCardell and Jim Bolton for their assistance in the design of the fixture and the experimental setup. This work was partially funded by the People Programme (Marie Curie Actions) of the European Union's Seventh Framework Programme (FP7/2007-2013) under REA grant agreement n. 299298. The results included here are the interpretation solely of the authors and do not represent necessarily the position of the funding agency.

VII. REFERENCES

[1] Alem NM, Bowman BM, Melvin JW, Benson JB. Whole Body Human Surrogate Response to Three-Point Harness Restraint. *Society of Automotive Engineers*, 1978. SAE No. 780895.

[2] Shaw G, Crandall J, Butcher J. Biofidelity evaluation of the Thor advanced frontal crash test dummy. *Proceedings of IRCOBI Conference,* 2000, Montpellier, France.

[3] Shaw G, Kent R, Sieveka E, Crandall J. Spinal kinematics of restrained occupants in frontal impacts. *Proceedings of IRCOBI Conference,* 2001, Isle of Man, United Kingdom.

[4] Lopez-Valdes F, Lau A et al. Analysis of spinal motion and loads during frontal impacts. Comparison between PMHS and ATD. *Annu Proc Assoc Adv Automot Med,* 2010, 54:61-78.

[5] Beeman SM, Kemper AR, Madigan ML, Franck CT, Loftus SC. Occupant kinematics in low-speed frontal sled tests: Human volunteers, Hybrid III ATD, and PMHS. *Accident Analysis and Prevention*, 2012, 47:128-139.

[6] Sherwood CP, Shaw CG, et al. Prediction of cervical spine injury risk for the 6-year-old child in frontal crashes. *Traffic Injury Prevention*, 2003, 4(3):206-213.

[7] Ash J, Sherwood C, et al. Comparison of anthropomorphic test dummies with a pediatric cadaver restrained by a three-point belt in frontal sled tests. *Proc 21st Enhanced Safety of Vehicles (ESV) Conference*, 2009, Stuttgart, Germany.

[8] Lopez-Valdes F, Forman J, Kent R, Bostrom O, Segui-Gomez M. A comparison between a child size PMHS and the Hybrid III 6 YO in a sled frontal impact. *Annu Proc Assoc Adv Automot Med*, 2009, 53:237-46.

[9] Seacrist T, Arbogast KB, et al. Kinetics of the cervical spine in pediatric and adult volunteers during low speed frontal impacts. *J Biomech*. 2012, 45(1):99-106.
[10] Seacrist T, Balasubramanian S, et al. Kinematic comparison of pediatric human volunteers and the Hybrid III 6-Year-Old Anthropomorphic Test Device. *Ann Adv Automot Med*. 2010, 54:97-108.
[11] Sran MM, Khan KM, Zhu Q and Oxland TR. Posteroanterior stiffness predicts sagittal plane midthoracic range of motion and three-dimensional flexibility in cadaveric spine segments. *Clin. Biomech. (Bristol., Avon.)*, 2005, 20(8):806-812.
[12] Anderson AL, McIff TE, Asher MA, Burton DC and Glattes RC. The effect of posterior thoracic spine anatomical structures on motion segment flexion stiffness. *Spine (Phila Pa 1976)*, 2009, 34(5):441-446.
[13] Markolf RL. Stiffness and damping characteristics of the thoracic-lumbar spine. *Proc. Workshop on Bioengineering Approaches to the Problems of the Spine*. 1970. NIH
[14] Panjabi M, Brand R, White A. Three dimensional flexibility and stiffness properties of the human thoracic spine. *Journal of Biomechanics*, 1976, 9:185-192.
[15] Willems JM, Jull GA, KF J. An in vivo study of the primary and coupled rotations of the thoracic spine. *Clin. Biomech.* (Bristol., Avon.), 1996, 11(6):311-316.
[16] Wachowski M, Mansour M, et al. How do spinal segments move? *J. Biomechanics*, 2009, 42:2286-2293.
[17] Lopez-Valdes FJ, Riley PO, et al. The six degrees of freedom motion of the human head, spine, and pelvis in a frontal impact. *Traffic Injury Prevention*, 2014, 15(3):294-301.
[18] Combest J. Status of the Global Human Body Models Consortium (GHBMC). *4th International Sysmposium on Human Modeling and Simulation in Automotive Engineering.* 2013. Available at: www.ghbmc.com. Accessed: March 27th, 2014.
[19] Kumaresan S, Yoganandan N, et al. Age-specific pediatric cervical spine biomechanical responses: three dimensional nonlinear finite element models. *Proceedings from the 41st Stapp Car Crash Conference.* 1997, Lake Buena Vista (FL), USA.
[20] Kumaresan S, Yoganandan N, et al. Biomechanical study of pediatric human cervical spine: a finite element approach. *J Biomech Eng,* 2000 122:60-71.
[21] Kumaresan S, Yoganandan N, et al. Biomechanics of pediatric cervical spine: compression, flexion and extension responses. *Traffic Inj Prev*, 2000, 2:87-101.
[22] Yoganandan N, Kumaresan S, Pintar FA. Biomechanics of the cervical spine part 2. Cervical spine soft tissue responses and biomechanical modeling. *Clin Biomech*, 2001, 16:1-27.
[23] Yoganandan N, Kumaresan S, et al. Pediatric Biomechanics. In: Nahum A, Melvin JW (eds). *Accidental injury: biomechanics and prevention.* 2002. Springer-Verlag, New York.
[24] Arbogast KB, Balasubramanian S, et al. Comparison of Kinematic Responses of the Head and Spine for Children and Adults in Low-Speed Frontal Sled Tests. *Stapp Car Crash J.* 2009, 53:329-72.
[25] Lopez-Valdes FJ, Seacrist T, et al. A methodology to estimate the kinematics of pediatric occupants in frontal impacts. *Traffic Injury Prevention.* 2012, 13(4):393-401.
[26] Nightingale RW and Luck JF. Experimental Injury Biomechanics of the Pediatric Neck. In: Crandall JR, Myers BS, Meaney DF, Zellers Schmidtke S. (eds) *Pediatric Injury Biomechanics,* 2013, Springer, New York.
[27] Center for Applied Biomechanics. Protocol for the Handling of Biological Material. 2006. Charlottesville, VA.
[28] Wu G, Siegler S, et al. ISB recommendation on definitions of joint coordinate system of various joints for the reporting of human joint motion- part I: ankle, hip and spine. *Journal of Biomechanics*, 2002, 35:543-548.
[29] Kinzel GL, Hall Jr AS, Hillberry BM. Measurement of the total motion between two body segments—I. Analytical development. *Journal of Biomechanics,* 1972, 5:93-105.
[30] Fung Y. 1993. Biomechanics: Mechanical properties of living tissues. Ed. Springer-Verlag.
[31] Funk J, Hall G, Crandall J, Pilkey W. Linear and quasi-linear viscoelastic characterization of ankle ligaments. *J Biomech Eng*, 2000, 122:15-22.
[32] Kent R, Bass C, Woods W, Sherwood C, Madeley N, Salzar R, Kitawaga Y. Muscle tetanus and loading conditions effects on the elastic and viscous characteristics of the thorax. *Traffic Injury Prevention,* 2003, 4:297-314.
[33] Kent R, Woods W, Bass C, Salzar R, Damon A. The transient relationship between pressure and volume in the pediatric pulmonary system. *Journal of Biomechanics*, 2009.
[34] Lucas SR, Bass CR, Crandall JR, Kent RW, Shen FH, Salzar RS. Viscoelastic and failure properties of spine ligament collagen fascicles. *Biomechanics and Modeling in Mechanobiology*, 2009.
[35] Salzar RS, Bass CR, Lessley D, Crandall JR, Kent RW, Bolton JR. Viscoelastic response of the thorax under dynamic belt loading. *Traffic Injury Prevention*, 2009, 10:290-296.

[36]Lopez-Valdes FJ, Lau S, Riey P, Lamp J, Kent R. The biomechanics of the pediatric and adult human thoracic spine. *Annals of Advances in Automotive Medicine*, 2011, 55:193-206.
[37]Yoganandan N, Arun MWJ, Stemper BD, Pintar FA, Maiman DJ. Biomechanics of human thoracolumbar spinal column trauma from vertical impact loading. *Annals of Advances in Automotive Medicine*, 2013, 57:155-166.
[38]El-Khoury GY and Whitten CG. Trauma to the upper thoracic spine: anatomy, biomechanics, and unique imaging features. *AJR American Journal of Roentgenology*, 1993, 160:95-102.
[39]Franklyn M, Peiris S, Huber C, Yang K. Pediatric material properties: a review of human child and animal surrogates. *Critical Reviews in Biomedical Engineering,* 2007, 35:197-342.
[40]Green NE, Swiontkowski MF. Skeletal trauma in children - Vol III. W.B. Saunders Company, Pennsylvania, 1998.
[41]Moore KL. and Dalley AF. Clinically Oriented Anatomy, 5th edition. Lippincott Williams and Wilkins, 2005.
[42]Ouyang J, Zhu Q, Zhao W, Xu Y, Chen W, Zhong S. Biomechanical assessment of the pediatric cervical spine under bending and tensile loading. *Spine*, 30(24):716-723.
[43]Hilker CE, Yoganandan N, Pintar FA. Experimental determination of adult and pediatric neck scale factors. *Stapp Car Crash Journal*, 2002, 46:417-429.
[44]Nightingale RW, Chancey VC, et al. Flexion and extension structural properties and strengths for male cervical spine segments. *Journal of Biomechanics*, 2007, 40:535-542.
[45]Nightingale RW, Winkelstein BA, Knaub KE, Richardson WJ, Luck JF, Myers BS. Comparative strengths of the upper and lower cervical spine in flexion and extension. *Journal of Biomechanics,* 2002, 35:725-732.
[46]Adams MA, Dolan P. Time-dependent changes in the lumbar spine's resistance to bending. *Clinical Biomechanics,* 1996, 119(4):194-200.
[47]Gardner-Morse MG, Stokes IAF. Structural behavior of human lumbar spinal motion segments. *Journal of Biomechanics,* 2004, 37:205-212.

VIII. APPENDIX

Quasi-linear Viscoelastic description of the bending behavior of a structure

As explained in the body of the paper, the selected QLV formulation related the calculated specimen angle to the generated bending moment, according to Eq. (1):

$$M(t) = \int_{-\infty}^{t} G(t-\tau)\left(\frac{\partial M_e(\alpha\alpha}{\partial \alpha}\right)\left(\frac{\partial \alpha(\tau)}{\partial \tau}\right)d\tau \quad (1)$$

The reduced relaxation function (G(t)) was described as the Prony series shown in Eq. (2):

$$G(t) = \sum_{i=1}^{3} G_i e^{-\beta_i t} + G_\infty \quad (2)$$

where β_i are time constants with associated weights G_i, and G_∞ the steady-state response. The maximum value of the reduced relaxation function occurs at time t=0 and is equal to unity:

$$\sum_{i=1}^{3} G_i + G_\infty = 1 \quad (3)$$

A nonlinear equation was used to model the instantaneous elastic response (IER) $M_e(\alpha)$ as shown below:

$$M_e(\alpha) = A(e^{B\alpha} - 1) \quad (4)$$

A numerical convolution scheme was used to solve for the eight parameters (A, B, G_i, β_i) that model the response of the FSU. The convolution can be developed by discretizing the time step and stepping forward in time to determine the steady state of the moment at each time step (M_∞):

$$M_\infty(t+dt) = M_\infty(t) + G_\infty\left(M_e(t+dt) - M_e(t)\right)$$

(5)

and the transient component of the moment at each time step (M_i):

$$M_i(t+dt) = \psi_i M_i(t) + (1-\psi_i)\left(\frac{G_i}{\beta_i}\right)\left(\frac{M_e(t+dt) - M_e(t)}{dt}\right)$$

(6)

where:

$$\psi_i = e^{-\beta_i dt}$$

(7)

Then, the total change in moment at each time point is the sum of the two terms, as shown in Eq. (8):

$$M(t) = M_\infty(t) + \sum_{i=1}^{3} M_i(t)$$

(8)

Calculation of the magnitudes needed to calculate the QLV model of the thoracic spine

The fixture used in the experiments described in this manuscript was designed to apply a controlled rotation to the ends of the specimens and measure the subsequent generated moments at both locations. The following steps detail the process of obtaining all the relevant magnitudes involved in calculating the model parameters used in the QLV model fit:

1) Calculate the bending moment (M_S) and the shear force (V_S) at the distal and proximal ends of each FSU, for each dynamic tests. The free body diagram of the fixture is shown in Figure A1.

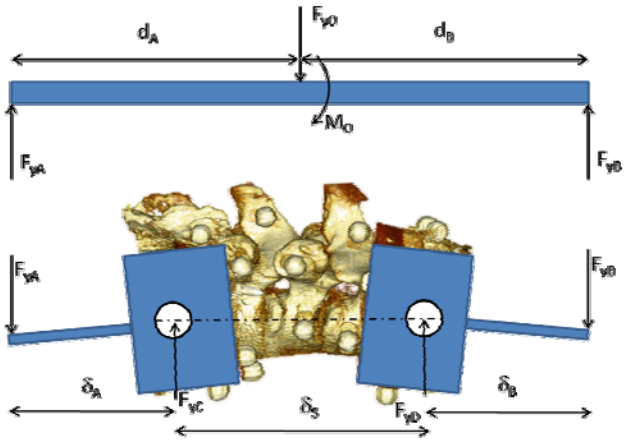

Fig. A1 Free body diagram of the fixture with the specimen.

2) All the distances in Fig. A1 were measured by the VICON system. The reactions F_{yA} and F_{yB} are the only forces that contribute to the moment generated at the pin joints C and D in the diagram above. The moment arms (δA and δB) were also measured during the tests. There is negligible horizontal force in the fixture due to the use of linear bearings connecting the fixture to the Instron crosshead and to the Instron table. F_{yC} and F_{yD} were measured directly by the two load cells. Therefore, the calculation to know the moment generated into the specimen relied only on obtaining the expression of F_{yA} and F_{yB} in terms of the known forces and distances. In the quasi-static case, these relationships can be easily obtained from the static equilibrium:

$$F_{yA} + F_{yB} = F_{yC} + F_{yD}$$

$$F_{yA} = \frac{F_{yD}\delta_B + F_{yC}(\delta_B + \delta_S)}{\delta_B + \delta_S + \delta_A}$$

(9)

However, the results presented in this manuscript correspond to dynamic tests and therefore Equation A1.6 might not be valid in this case. The following analysis shows that the contribution of the inertia to the calculation of the forces is so small that the equations derived for the quasi-static conditions can still be used in

the dynamic case. Fig. A2 shows the free body diagram corresponding to one of the rotating cups, considering the reactions of the specimen on the cup.

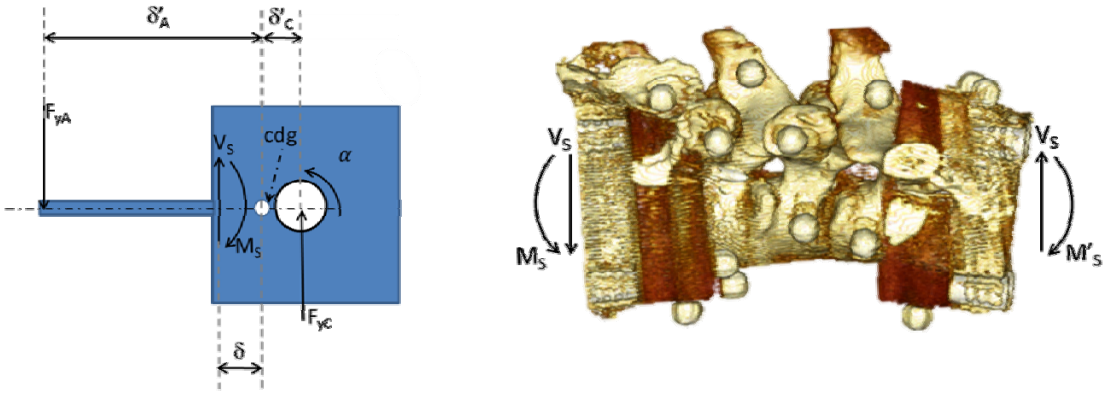

Fig. A2 Free body diagram of the fixture with the specimen.

In the dynamic case, the equations of motion are given by Eq. (10), where Vs and Ms are the shear and moment reactions of the specimen on the cup:

$$F_{yA} - F_{yC} - V_s = m\ddot{y}_{cdg}$$
$$-F_{yA}\delta'_A + V_s\delta + M_s - F_{yC}\delta'_C = I_{cdg}\alpha$$
(10)

The total mass of the cup and the lever is 0.114 kg and a representative value of the vertical acceleration of the center of gravity of the assembly is about 0.00525 m/s^2 (the distance between the pivot C and the center of gravity of the assembly is 3 mm). The magnitude of the inertial contribution to the force equation is several orders of magnitude smaller than the resolution of the load cell and can be neglected. A similar reasoning can be applied to the inertial term in the moments equation (I_{cdg}=A1.32e-4 kgm^2; α=67.7 rad/s^2) and again the inertia contribution to the moments equation is several orders of magnitude smaller than the contribution of the other moments. Thus, the inertial term can be neglected in both Eq. (10) and the expressions to calculate F_{yA} and F_{yB} given in Eq. (9) are valid. These expressions allow calculating the moment generated in the specimen by the rotation of the cups.

The asymmetrical nature of the specimen caused that specimens were subjected also to shear loads. However, Eq. (10) can also help to estimate the magnitude of the shear applied to the specimen as the difference between F_{yA} and F_{yC}, and the subsequent bending moment at each of the ends of the specimen:

$$V_s = F_{yA} - F_{yC}$$
$$M_s = F_{yA}\delta'_A - V_s\delta_s + F_{yC}\delta'_C$$
(11)

3) Calculate the bending moment at the center of each vertebra (M_{Oi}) using the distances measured by the Vicon system.

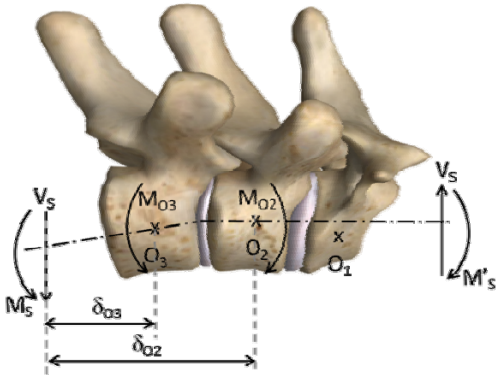

$$M_{O3} = M_s + V_s\delta_{O3}$$
$$M_{O2} = M_s + V_s\delta_{O2}$$
(12)

Fig. A3 Schematic showing the bending moments MOi at the center of

the vertebrae and the parameters involved in the calculations.

4) Average the bending moments calculated at the center of contiguous vertebrae:

$$M_{32} = \frac{1}{2}\left(M_{O3} + M_{O2}\right) \quad (13)$$

5) Calculate the relative rotation between contiguous vertebrae in the sagittal plane. After this step, there will be two values of the average moment and the relative angle per FSU, corresponding to the superior and inferior aspect of the specimen.

6) Input each of the previously obtained average moments (M_{32}) and relative angle pair into the de-convolution MATLAB script.

7) Obtain the value of the QLV model parameters that minimize the square standard error between the modeled moment and the average one (M_{32}). Only the tests with amplitudes D3, D4 and D5 were used in the calculation of the model. The optimization of the parameters was done using a genetic algorithm method and the results for the three different amplitudes were considered in a single optimization process. It was found that the solutions provided by other solvers implemented in MATLAB were extremely dependent on the initial guess value and frequently the solution obtained was a local minimum instead of a global one. The constraints used in the optimization were:

a. All the parameters should be positive.

b. $\sum_{i=1}^{3} G_i < 1$

c. The parameter values were contained within the intervals shown in Table A1:

TABLE A1
BOUNDS USED IN THE OPTIMIZATION OF THE MODEL PARAMETERS

	Lower bound	Upper bound
β1 (s)	0.0001	10
β2 (s)	0.001	100
β3 (s)	0.01	1000
G1	0.000001	1
G2	0.000001	1
G3	0.000001	1
A	1	10000
B	0.0001	1

Geometry of the FSU

The most relevant geometrical characteristics of the vertebrae of each specimen are included in Table A2 and Table A3. Dimensions in the table correspond to the magnitudes indicated in the schematic shown in Fig. A4.

TABLE A2
GEOMETRY OF THE VERTEBRAE OF T2-T4 SPECIMENS AS DEFINED IN FIG. A4

	F470	M485	M319	M320
Curvature (deg)	175.29	181.87	-	-
T2 height (mm)	6.62	17.24	-	-
T3 height(mm)	6.82	18.51	-	-
T4 height(mm)	6.21	18.00	-	-
T2-T3 iv disc height (mm)	7.91	4.82	-	-
T3-T4 iv disc height (mm)	7.51	5.07	-	-
T2 width (mm)	22.81	27.97	-	-
T3 width(mm)	21.56	23.03	-	-
T4 width(mm)	20.72	24.04	-	-
T2 length (mm)	12.36	14.75	-	-
T3 length (mm)	13.82	13.24	-	-
T4 length (mm)	14.24	20.18	-	-
T2-T3 facet angle, right (deg)	57.85	79.64	-	-
T2-T3 facet angle, left (deg)	66.84	73.33	-	-
T3-T4 facet angle, right (deg)	42.56	70.59	-	-
T3-T4 facet angle, left (deg)	67.56	81.89	-	-

TABLE A3
GEOMETRY OF THE VERTEBRAE OF T7-T9 SPECIMENS AS DEFINED IN FIG. A4

	F470	M485	M319	M320
Curvature (deg)	183.18	183.00	176.56	179.24
T7 height (mm)	7.55	16.53	20.43	19.54
T8 height(mm)	8.24	20.66	21.29	19.81
T9 height(mm)	7.55	20.66	22.73	20.34
T7-T8 iv disc height (mm)	7.78	8.26	4.03	5.62
T8-T9 iv disc height(mm)	6.86	6.71	6.91	6.42
T7 width (mm)	22.78	26.42	25.23	26.64
T8 width(mm)	21.52	27.26	26.87	27.79
T9 width(mm)	22.49	26.20	26.97	29.68
T7 length (mm)	16.32	23.23	25.56	25.08
T8 length(mm)	15.47	24.92	26.23	28.38
T9 length(mm)	16.24	25.77	28.39	29.32
T7-T8 facet angle, right (deg)	41.69	83.30	79.61	59.08
T7-T8 facet angle, left (deg)	76.53	82.58	86.02	68.24
T8-T9 facet angle, right (deg)	72.38	79.10	85.43	62.86
T8-T9 facet angle, left (deg)	71.60	79.24	89.91	65.14

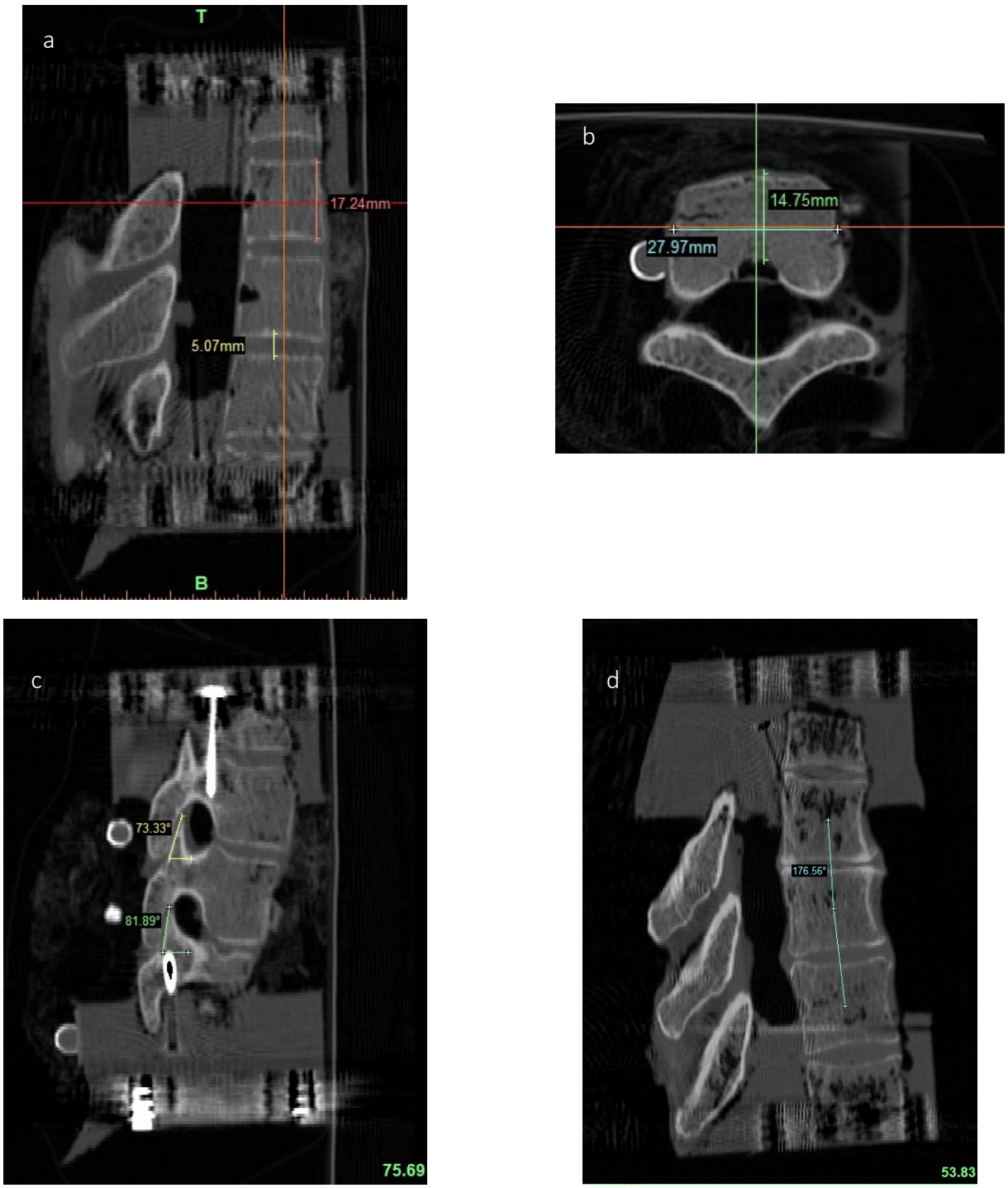

Fig. A4 Schematic showing the parameters of the vertebrae measured for each of the specimens:
a) Mid-sagittal view illustrating the height of the T2 vertebra measured at the anterior aspect and the measurement of the T3T4 intervertebral disc height at the maximum height of the disc. Specimen M485 T2T4.
b) Section of T2 at approximately mid height of the vertebral body, showing the measurement of the vertebra length (green dimension) and width (blue dimension). Specimen M485 T2T4.
c) Measurement of the facet angles with respect to the horizontal. Lateral view of specimen M485 T2T4, left aspect
d) Measurement of initial curvature in the sagittal plane. This section corresponds to the mid-sagittal plane. Angle measured between the segments connecting the approximate center of the vertebrae. CT image from M319 T7T9.

Responses of the specimens to the D3, D4 and D5 step and hold tests

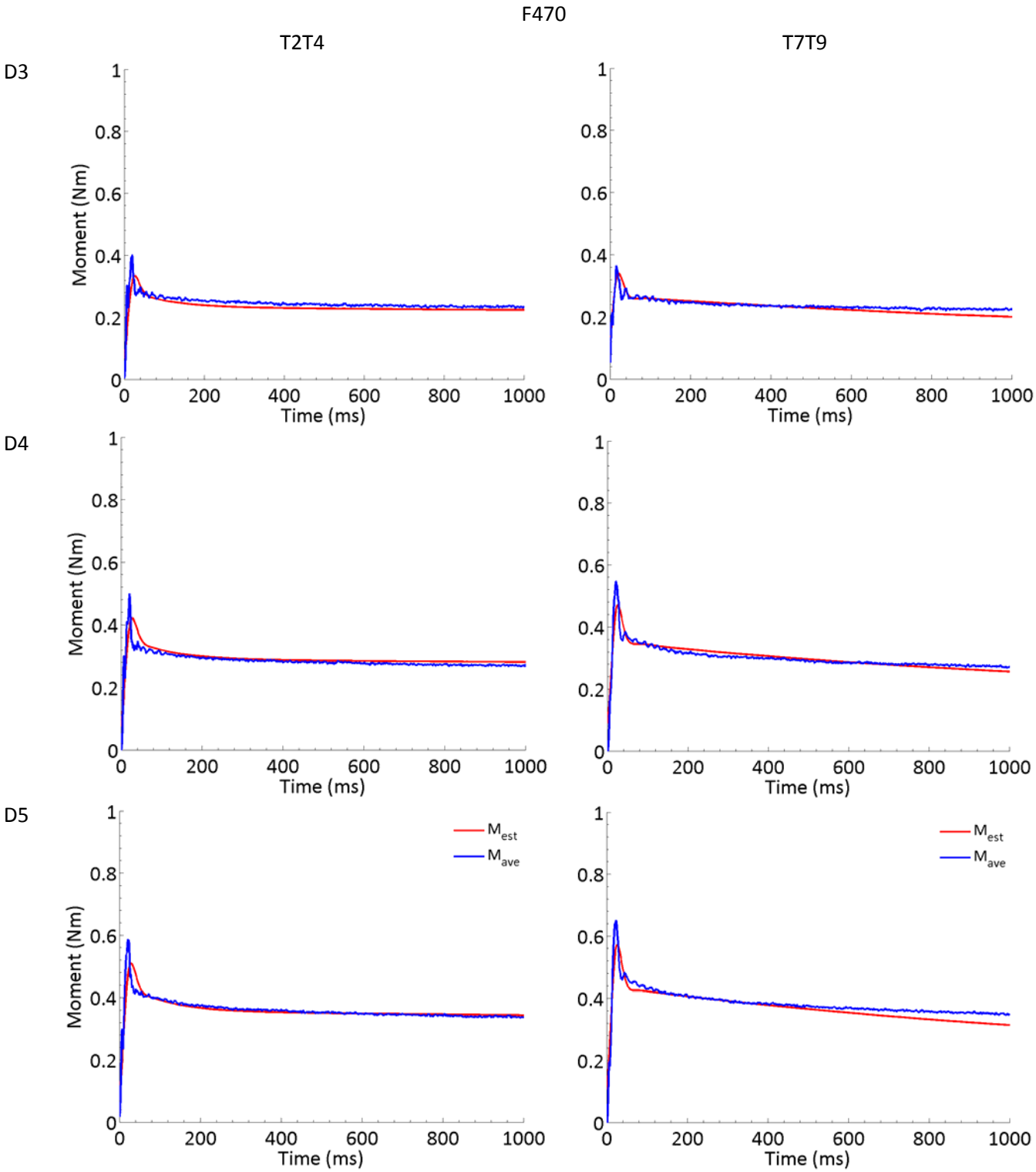

Fig. A5 Comparison between the measured moment (M_{ave}, blue) and the QLV-estimated moment (M_{est}, red). Specimen F470. Left column shows the T2-T4 section and right column corresponds to the T7-T9 section.

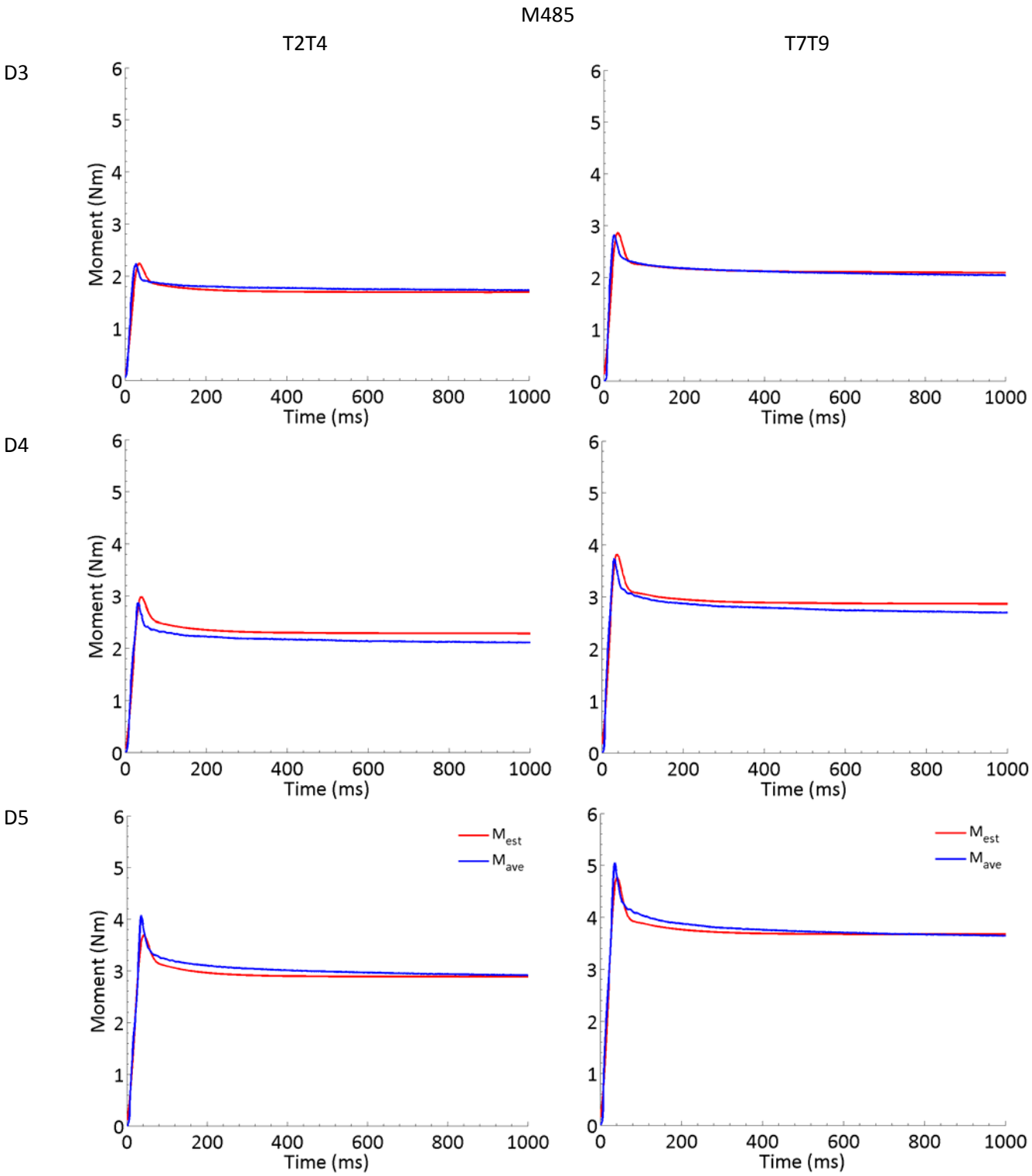

Fig. A6 Comparison between the measured moment (M_{ave}, blue) and the QLV-estimated moment (M_{est}, red). Specimen M485. Left column shows the T2-T4 section and right column corresponds to the T7-T9 section.

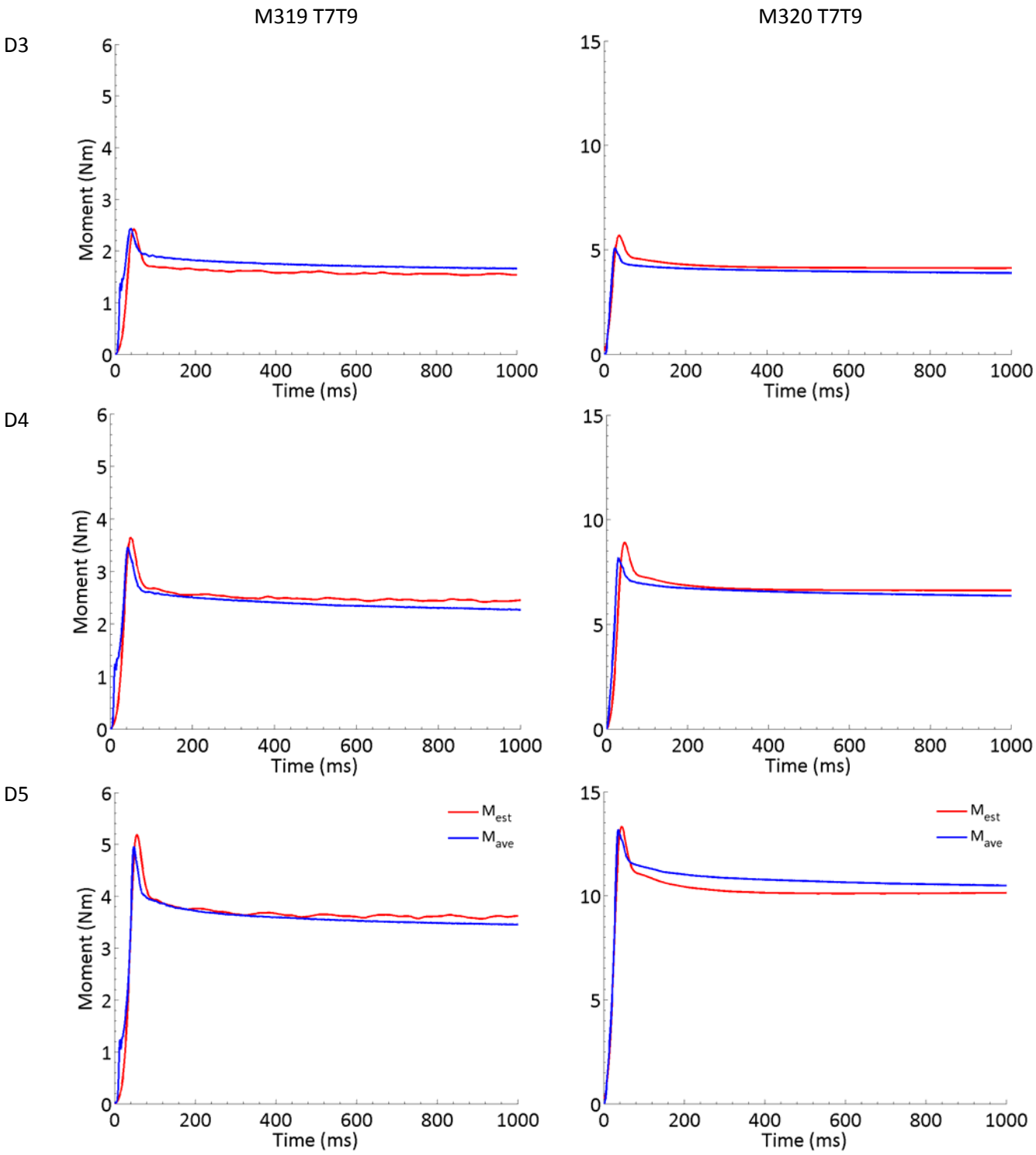

Fig. A7 Comparison between the measured moment (M_{ave}, blue) and the QLV-estimated moment (M_{est}, red). Specimen M319 T7T9 (left column) and specimen M320 T7T9 (right column).